AgriEngineering

MDPI

Article

Hyperspectral Response of the Soybean Crop as a Function of Target Spot (*Corynespora cassiicola*) Using Machine Learning to Classify Severity Levels

José Donizete de Queiroz Otone [1], Gustavo de Faria Theodoro [1], Dthenifer Cordeiro Santana [1], Larissa Pereira Ribeiro Teodoro [1], Job Teixeira de Oliveira [1], Izabela Cristina de Oliveira [1], Carlos Antonio da Silva Junior [2], Paulo Eduardo Teodoro [1,*] and Fabio Henrique Rojo Baio [1]

[1] Departament of Agronomy, Federal University of Mato Grosso do Sul (UFMS), Chapadão do Sul 79560-000, MS, Brazil; josedonizete.q.o@hotmail.com (J.D.d.Q.O.); gustavo.theodoro@ufms.br (G.d.F.T.); dthenifer.santana@unesp.br (D.C.S.); larissa_ribeiro@ufms.br (L.P.R.T.); job.oliveira@ufms.br (J.T.d.O.); izabela.oliveira@unesp.br (I.C.d.O.); fabio.baio@ufms.br (F.H.R.B.)

[2] Department of Geography, State University of Mato Grosso (UNEMAT), Sinop 78550-000, MT, Brazil; carlosjr@unemat.br

* Correspondence: paulo.teodoro@ufms.br

Citation: de Queiroz Otone, J.D.; Theodoro, G.d.F.; Santana, D.C.; Teodoro, L.P.R.; de Oliveira, J.T.; de Oliveira, I.C.; da Silva Junior, C.A.; Teodoro, P.E.; Baio, F.H.R. Hyperspectral Response of the Soybean Crop as a Function of Target Spot (*Corynespora cassiicola*) Using Machine Learning to Classify Severity Levels. *AgriEngineering* **2024**, *6*, 330–343. https://doi.org/10.3390/agriengineering6010020

Academic Editors: Jing Zhou and Lirong Xiang

Received: 28 November 2023
Revised: 19 January 2024
Accepted: 22 January 2024
Published: 7 February 2024

Abstract: Plants respond to biotic and abiotic pressures by changing their biophysical and biochemical aspects, such as reducing their biomass and developing chlorosis, which can be readily identified using remote-sensing techniques applied to the VIS/NIR/SWIR spectrum range. In the current scenario of agriculture, production efficiency is fundamental for farmers, but diseases such as target spot continue to harm soybean yield. Remote sensing, especially hyperspectral sensing, can detect these diseases, but has disadvantages such as cost and complexity, thus favoring the use of UAVs in these activities, as they are more economical. The objectives of this study were: (i) to identify the most appropriate input variable (bands, vegetation indices and all reflectance ranges) for the metrics assessed in machine learning models; (ii) to verify whether there is a statistical difference in the response of NDVI (normalized difference vegetation index), grain weight and yield when subjected to different levels of severity; and (iii) to identify whether there is a relationship between the spectral bands and vegetation indices with the levels of target spot severity, grain weight and yield. The field experiment was carried out in the 2022/23 crop season and involved different fungicide treatments to obtain different levels of disease severity. A spectroradiometer and UAV (unmanned aerial vehicle) imagery were used to collect spectral data from the leaves. Data were subjected to machine learning analysis using different algorithms. LR (logistic regression) and SVM (support vector machine) algorithms performed better in classifying target spot severity levels when spectral data were used. Multivariate canonical analysis showed that healthy leaves stood out at specific wavelengths, while diseased leaves showed different spectral patterns. Disease detection using hyperspectral sensors enabled detailed information acquisition. Our findings reveal that remote sensing, especially using hyperspectral sensors and machine learning techniques, can be effective in the early detection and monitoring of target spot in the soybean crop, enabling fast decision-making for the control and prevention of yield losses.

Keywords: disease monitoring; classification analysis; machine learning; precision agriculture; remote sensing

1. Introduction

The monitoring and mapping of crops on a large scale are essential to assist in management and decision-making in various crops, thus improving production efficiency in a more technological way [1,2]. In this context, remote sensing is an effective strategy, allowing better precision in agricultural monitoring, especially in the health of crops, such as soybeans, which are regularly affected by foliar diseases [3], which lead to irreversible economic damage.

One of the diseases that affects the soybean [*Glycine max (*L.) Merril] is target spot (*Corynespora cassiicola*), which has become increasingly prominent since 2010 due to the use of sensitive cultivars and loss of sensitivity to regulated fungicides. Several resistant strains of the fungus have emerged in recent years, increasing its spread and making control difficult, generating economic losses in several soybean production areas [4]. Some recent studies have reported yield losses of up to 24%. Among the factors that increase its importance, its ability to survive in crop residues has a major impact [5]. Another aspect of great importance for this disease is its host range, of which 530 plant species have been reported [6–9].

Plants respond to biotic and abiotic pressures by changing their biophysical and biochemical aspects, such as reducing their biomass and developing chlorosis, which can be readily identified using remote-sensing techniques applied to the visible, near-infrared and shortwave infrared spectrum range (VIS/NIR/SWIR) [10]. The early identification of crop diseases offers adequate time to control potential epidemics and minimize yield losses. In view of this, professionals in precision agriculture persist in the search for innovative and economical solutions that easily and effectively address disease detection [11]. Due to advances in technology, increasingly smaller, lighter and cheaper sensors have become available for remote-sensing drone applications. In the literature, it is possible to find detailed introductions to various drone remote-sensing systems [12,13].

A more sophisticated imaging technique, called hyperspectral imaging, uses reflectance data collected over a wide spectral range, usually between 350 and 2500 nm, in order to reconstruct a spatial representation of the plant leaf under analysis through highly specialized image processing procedures. Although the use of hyperspectral data is an extremely informative approach that enables the detection of a wider range of plant diseases compared to RGB imaging, it does have some disadvantages, including high costs, longer data acquisition periods and complex data analysis, especially in situations where rapid responses or extensive assessment of large areas are required [14]. In this sense, using machine learning techniques allied to remote sensing enables technological advances in the agricultural environment in crop monitoring, especially in phytosanitary aspects. The authors of [15] recommend the processing of sensor data by using machine learning for fast and accurate classification in crop diseases.

The hypothesis of this study is that it is possible to diagnose the occurrence of target spot on soybean leaves using hyperspectral and multispectral sensors, and to analyze the relationship between these spectral characteristics and the crop yield. The objectives of this study were: (i) identify spectral differences between target spot disease severity levels; (ii) investigate the relationship between disease severity levels and multi- and hyperspectral data; (iii) identify the best input that guarantees the best performance of machine learning algorithms between multi- and hyperspectral data.

2. Materials and Methods

2.1. Study Area

The study was carried out in the 2022/2023 crop season at Fazenda Nova França, at the geographical coordinates of 53°06′40.09″ W, 18°16′06.01″ S, in the municipality of Costa Rica, State of Mato Grosso do Sul, Brazil (Figure 1). According to Koppen classification, the region's climate is tropical humid (Aw), with a rainy season in summer and a dry season in winter. The soil is classified as dystrophic Red Latosol with a very clayey texture [16].

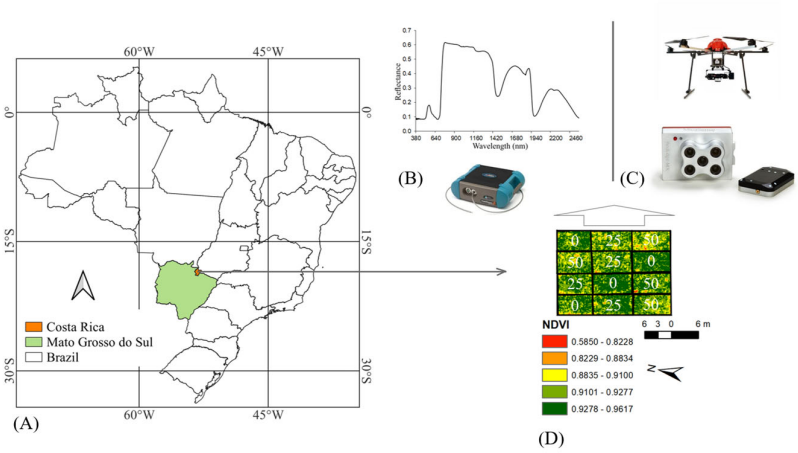

Figure 1. Location of the study area (**A**), equipment used in hyper (**B**) and multispectral (**C**) imagery, and diagram of the map of target spot severity obtained from NDVI index (**D**).

Figure 2 shows the climatic conditions of the experiment throughout the soybean crop cycle. The average temperature throughout the cycle was 21.39 °C and the average rainfall was 26.22 mm. There was a higher rainfall rate close to 40 days after plant emergence and mild temperatures, which favored the incidence of the disease and, as desired, provided suitable conditions for the treatments.

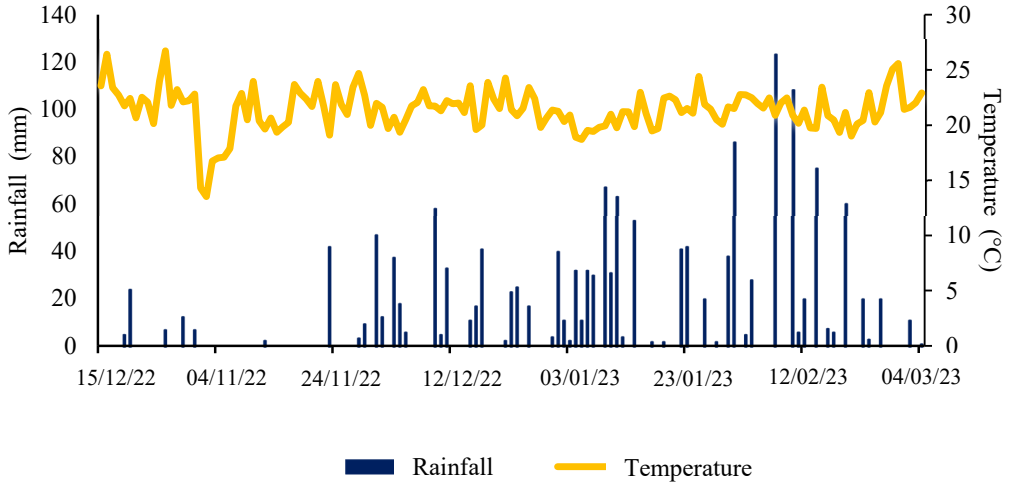

Figure 2. Average rainfall and temperature conditions during the experiment.

The experiment was carried out in an area that had cotton (*Gossypium hirsutum* L.) as a previous crop. Data obtained from the chemical analysis of the soil are shown in Table 1. Fertilization together with sowing was carried out by applying 171 kg ha^{-1} of NPK formulate 06-35-06 and 83 kg ha^{-1} of potassium chloride before sowing. Sowing was carried out on 15 October 2022, using the M 5947 IPRO soybean cultivar, which has INTACTA RR2 PRO technology and a relative maturity of 5.9, considered super early (3Tentos, Bárbara do Sul, Brazil). The sowing density adopted was eighteen plants m^{-1} and an initial population of 377,774 plants ha^{-1}. The seedlings emerged on 20 October 2022. During the experiment, all the cultural treatments and phytosanitary management were carried out according to recommendations for the crop, except for the application of fungicides, which was carried out according to the treatments [17]. The plots were composed of seven rows spaced 0.45 m apart and 5.5 m long, giving a total area of 17.3

m². The useful area used for data collection was 4.0 m of the two central rows of each plot, totaling 3.6 m².

Table 1. Chemical properties of the soil in the experimental area.

pH	H + Al	Ca	Mg	Al	CEC	B	Cu	Fe	Mn	Zn	K	P	OM	Clay	V	m
		cmolc dm^{-3}						mg dm^{-3}					g dm^{-3}		%	
5.3	4.6	5.5	1.7	0.05	12.0	0.33	1.4	45.0	16.6	5.2	97.0	37.4	36.1	67	60.2	0.8

pH $CaCl_2$; H + Al: potential acidity; Ca: calcium; Mg: magnesium; Al: aluminum; CEC: cation exchange capacity; B: boron; Cu: copper; Fe: iron; Mn: manganese; Zn: zinc; K: potassium; P: phosphorus (Mehlich); OM: organic matter; Clay: soil clay content; V: base saturation; m: aluminum saturation.

2.2. Experimental Design

Four experimental plots were set up per treatment, in which the plants were treated with different fungicides, where we considered Treatment 1 to be 50% of the leaf area damaged by the disease where no fungicide was applied. We chose Treatment 2 with 25% of the leaf area damaged, where Pyraclostrobin + Fluxapiroxad (116.55 + 58.45 g of active ingredient per ha^{-1}) was applied, and Treatment 3 with healthy leaves, without symptoms of the disease, obtained by spraying Azoxystrobin + Prothioconazole + Mancozeb (75 + 1050 + 75 g of active ingredient per ha^{-1}). These sprayings were carried out at intervals (15 days after application—DAA) starting at 30 days after emergence (DAE), adding up to 3 applications over the crop cycle. The spraying of each treatment was carried out with the aim of inducing the onset of the disease for spectral measurement of severity levels.

On 18 January 2023, when the crop was in phenological stage R5.5 (grain filling—76 to 100% graining—in one of the four upper nodes on the main stem), the leaves were collected from the plots of the different treatments, where 100 healthy leaflets, 100 leaflets with 25% severity and 100 leaflets with 50% severity were obtained (Figure 3), based on the diagrammatic scale drawn up by [18]. These samples were identified and transported in a polystyrene box from the field to the laboratory so that the turgidity of the leaflets was maintained.

(**A**) (**B**) (**C**)

Figure 3. Healthy leaves (**A**), leaves with 25% target spot severity (**B**), and leaves with 50% target spot severity (**C**).

2.3. Spectral Analysis

The hyperspectral sensor analyses of each soybean leaf sample were carried out in the laboratory of the Federal University of Mato Grosso do Sul (campus of Chapadão do Sul), Brazil, using the FieldSpec 4 HRes spectroradiometer from Analytical Spectral Devices (ASD, London, UK). This equipment can carry out spectral measurements over a wide range from 350 to 2500 nm. Readings were recorded with an interval of 1.4 nm in the 50 to 1050 nm range and 2 nm in the 1000 to 2500 nm range. The samples were measured

using the optional ASD Plant Probe reader (ASD, London, UK). One of the main advantages of this option is that the spectral reading is not affected by the ambient light. Using recommendations from [19], the spectral reading peaks related to the main plant physiological characteristics and are described in Table 2.

Table 2. Spectral band center as a function of plant characteristics.

Spectral Band Center (nm)	Plant Physiological Characteristics
370	Phototropism
420	a-carotene
425	b-carotene
430	Chlorophyll absorption
440	a-carotene
445	xanthophyll
445	Chlorophyll synthesis
450	b-carotene
453	Chlorophyll b
470	a-carotene
475	Chlorophyll b
480	a-carotene
650	Chlorophyll synthesis
960	Chlorophyll absorption
1100	Chlorophyll absorption
1400	Water absorption
1930	Water absorption
2200	Al-OH, Mg-OH and CO_3 peak

Ref [19].

The spectral bands of the repetitions in each treatment were extracted in order to assess the best characterization of the disease in relation to spectral characteristics (whether by spectral bands, vegetation indices [VIs], or by the direct reflectance of the sensor) and phenological characteristics. The spectral bands were defined based on the reflectance peaks of the electromagnetic spectrum in the identification of plant physiological characteristics (Table 2). The spectral bands were calculated according to the methodology described by [19] using the values obtained by calculating the difference between the reflectance values at the point of least inflection and the point of greatest subsequent range. The ranges of the bands used are described in Table 3.

Table 3. Intervals of the electromagnetic spectrum in each band analyzed.

Band	Spectral Range (nm)
B1	390–420
B2	435–470
B3	480–550
B4	555–670
B5	680–750
B6	755–970
B7	1070–1120
B8	1270–1430
B9	1460–1650
B10	1850–1930
B11	2130–2460

On 20 January 2023, at 90 DAE, with the crop at reproductive stage R5.5, spectral images were acquired by a remotely piloted aircraft (RPA) used as an aerial platform for the multispectral sensor. RPA XFly X800 was equipped with a Micasense multispectral camera, model Red-edge MX with 1280 × 960 pixels and with a spatial resolution in the scene corresponding to 0.06 m (in each band). The system mapped images in the blue (B) (475 nm center, 20 nm bandwidth), green (G) (560 nm center, 20 nm bandwidth), red (R) (668 nm center, 10 nm bandwidth), red edge (RE) (717 nm center, 10 nm bandwidth), and near-infrared (NIR) (840 nm center, 40 nm bandwidth) bands. The overflight was carried out at a 60 m altitude. The images were orthorectified using the Pix4D program version 1.55 Radiometric correction was carried out based on a standard reflective target. The maps were manipulated and the vegetation indices extracted from the respective plots using the ArcGis software version 10.5. The characterizations of these vegetation indices are shown in Table 4.

Table 4. Vegetation indices calculated from reflectance values in the red (668 nm), green (560 nm), red edge (717 nm), Nir (840 nm) and blue (475 nm) spectral bands collected by the multispectral camera.

Abbreviation	Vegetation Index	Equation	Reference
NDVI	Normalized difference Vegetation index	$\frac{(Nir - R)}{(Nir + R)}$	[20]
NDRE	Normalized difference Red edge index	$\frac{(Nir - RE)}{(Nir + RE)}$	[21]
SAVI	Soil-adjusted Vegetation index	$(1 + 0.5) \times \frac{(Nir - R)}{(Nir + R + 0.5)}$	[22]
GNDVI	Green normalized Difference vegetation	$\frac{(Nir - G)}{(Nir + G)}$	[23]
EVI	Enhanced vegetation Index	$\frac{(Nir - R)}{((Nir + (6 \times R) - (7.5 \times B) + 1))}$	[22]
MCCI	Modified canopy Chlorophyll content index	$\frac{NDRE}{NDVI}$	[24]

Nir: near-infrared reflectance; R: red reflectance; RE: red edge reflectance; G: green reflectance; B: blue reflectance.

2.4. Data Analyses

By sowing with an early-cycle cultivar, we were able to isolate the target spot factor without the presence of other diseases. Data obtained from reflectance bands and vegetation indices were submitted to machine learning analysis (Table 5); the algorithms were selected because they are most used in agriculture for various tasks. The parameters were adjusted according to the default settings in the Weka 3.8.5 software. The ANN used was of the multilayer perceptron type using a backpropagation algorithm to adjust the weights of the neural network connections with learning rates equal to 0.3, moment rates equal to 0.2 and 500 epochs, containing 10 neurons in the first layer and 10 neurons in the second. The J48 algorithm is an adaptation of the C4.5 classifier and can be used in various classification and prediction tasks, with a pruning procedure being adopted and the minimum number of instances allowed in a leaf node adopted was equal to 4. REPTree is a model similar to the decision tree, which generates several trees in different interactions, selecting the best tree using information gain and performing error reduction pruning such as split classifications. RF produces multiple prediction trees for the same dataset and uses a voting scheme among all learned trees to predict new values. SVM performs classification tasks by building hyperplanes in a multidimensional space to distinguish different classes

Table 5. Machine learning models used in classification.

ML	Machine Learning Model	Reference
ANN	Multilayer perceptron artificial neural network	[25]
J48	J48 decision tree	[26]
RL	Logistic regression	[27]
DT	REPTree decision tree	[28]
RF	Random forest	[29]
Rt	Random tree decision tree	[30]
SVM	Support vector machine	[31]

The effectiveness of the machine learning model was evaluated using performance metrics, including the correct classification percentage (CC), F-score and the Kappa coefficient (Table 6). The performance of the models was then subjected to an analysis of variance to determine whether there were significant differences between the variables and the machine learning models, as well as to assess the interaction between them.

Table 6. Accuracy of the algorithms and their respective equations.

Abbreviation	Accuracy	Equation
CC	Correct classifications	$\boldsymbol{CC = \frac{(number\ of\ correct\ predictions)}{(total\ instances)}}$
F-score	F-score	$\boldsymbol{\frac{2 \times (Precision \times recall)}{(Precision + recall)}}$
Kappa	Kappa coefficient	$\boldsymbol{Kappa = \frac{(observed\ agreement — agreement\ expected\ by\ chance)}{(1 - \text{agreement expected by chance})}}$

The metrics were subjected to analysis of variance, and when significant differences were obtained, boxplots were generated to visualize the means, grouped by the Scott–Knott test at 5% significance level. All the bands, vegetation indices and yield data obtained from plots with healthy leaves and 25 and 50% severity levels were subjected to multivariate canonical analysis. The grouping of means by Scott–Knott and canonical variables were carried out using the Rbio software [32], while the boxplots were generated using the ggplot2 and ExpDes.pt packages on the R software version 4.1.0.

3. Results

Disease severity levels showed different hyperspectral curves (Figure 4). It is remarkable that the highest reflectance in the visible region occurred in the highest severity leaves (50%), while the lowest reflectance was in the healthy leaves, especially in the 508–700 nm wavelengths corresponding to bands B3, B4 and B5.

Healthy leaves showed similar reflectance at a severity level of 25% in the wavelength range from 725 to 863 nm, from which point there was a decrease in reflectance up to the short-wave infrared (SWIR) region. In the near-infrared (NIR) region, 50% severity showed low reflectance between the wavelengths from 725 to 794 nm, with a subsequent increase in reflectance from this point up to the SWIR bands. This behavior was notably represented by bands B6, B7 and B8, corresponding directly to the water content in the leaves. Meanwhile, the 25% severity level revealed an increase in reflectance in the 725 to 1346 nm range, showing intermediate reflectance in the SWIR region.

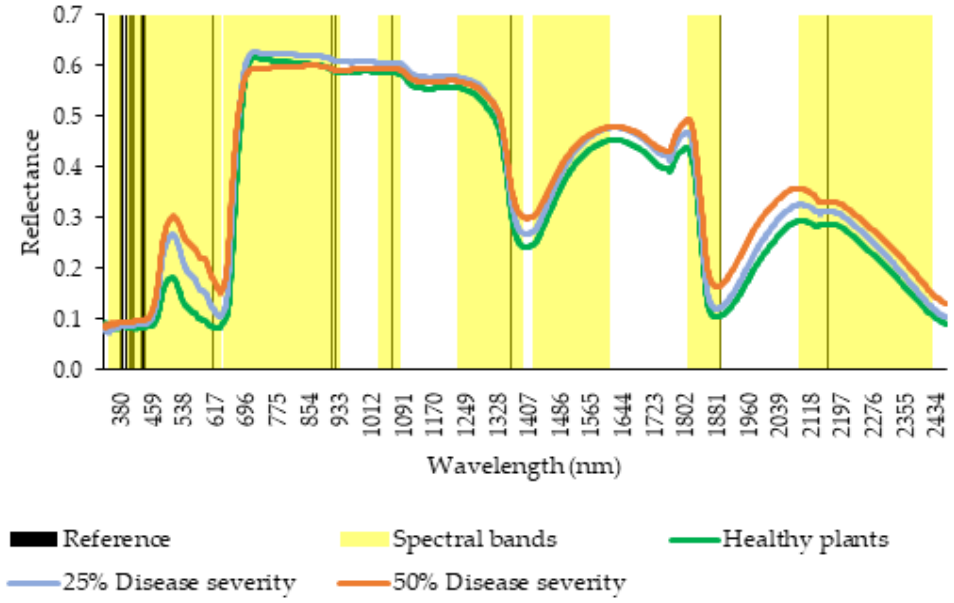

Figure 4. Spectral signature for each level of target spot severity in soybean.

Canonical analysis revealed a closer relationship between healthy leaves and NDRE and GNDVI (Figure 5A). Leaves with 25% severity were close to the 680–750 nm, and 1460–1650 nm bands. More severely attacked leaves were close to the 435–470 nm, 2130–2460 nm, and 1850–1930 nm ranges, where the wavelengths presented an increase in reflectance at these levels of severity (Figure 4).

Figure 5B shows that healthy leaves and yield were closest to the SAVI, EVI, 840 nm and grain weight vectors. Leaves with 25% severity were close to 475 nm, 560 nm, 668 nm, and 717 nm wavelengths.

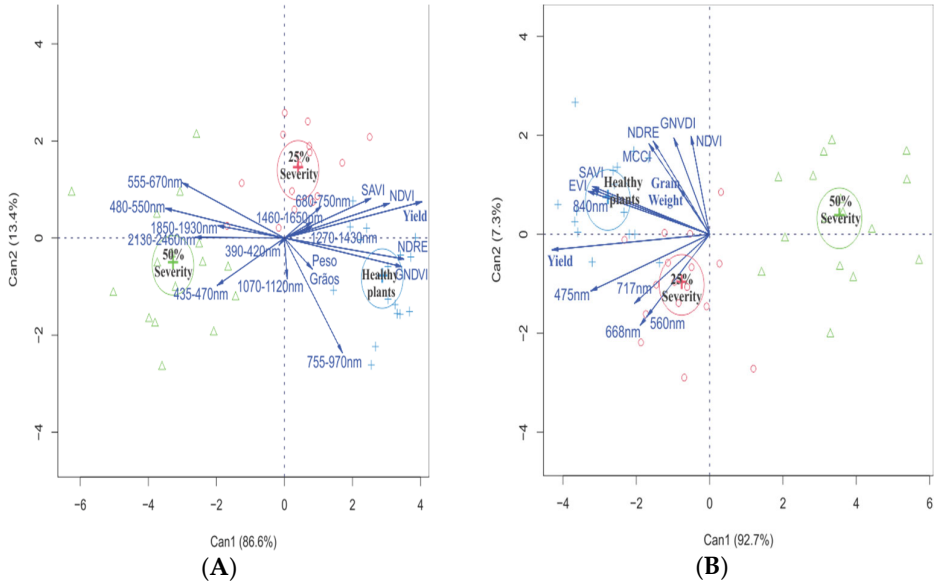

Figure 5. Canonical analysis relating spectral bands based on a hyperspectral sensor (**A**) and vegetation indices based on a multispectral sensor (**B**) with the levels of target spot severity, grain yield, and grain weight.

Overall, the levels of disease severity differed from each other and formed different spectral signatures. Thus, data were submitted to machine learning (ML) analysis in order to find the best algorithm for classifying target spot severity levels in soybean. Six ML algorithms and three different input configurations were used, resulting in a significant interaction between them for the three accuracy metrics tested: correct classification percentage (CC), F-score, and Kappa.

For the CC and Kappa metrics (Figure 6), when using the bands as input configuration, the best performance was achieved by LR and ANN. When using VIs as input, ANN outperformed the other algorithms. Using all the reflectance values provided by the sensor, LR and SVM showed the highest accuracies. When comparing the three inputs within the algorithms, all had the best performance when using all the reflectance information from the sensor.

Considering the F-score metric using bands as input, the best performances were achieved by the RF, LR, ANN and SVM algorithms (Figure 6). Using VIs as input, LR and ANN showed the best responses. Using all the information provided by the sensor, LR and SVM had the best results. Comparing the three inputs within each algorithm, J48, RF and RNA were better using the bands. REPtree and LR had similar performances using bands or reflectance. SVM achieved better accuracy using reflectance as input.

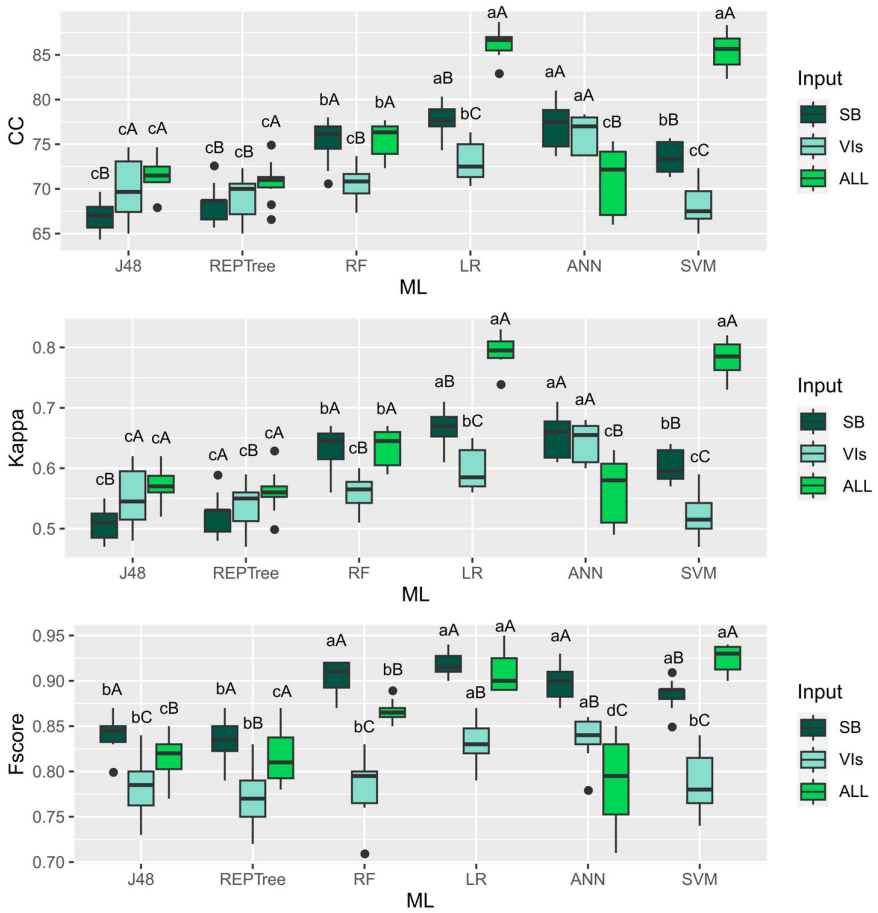

Figure 6. Boxplots for the accuracy metrics correct classification percentage (CC), Kappa, and F-score considering the machine learning models and different inputs tested for classifying target spot severities in soybeans in 100 samples for each severity. SB: spectral bands; VIs: vegetation indices; ALL: all reflectance ranges provided by the hyperspectral sensor. Averages followed by the same uppercase letters for the different inputs and the same lowercase letters for the different ML algorithms do not differ by the Scott–Knott test at 5% probability.

4. Discussion

The biophysical and biochemical behavior of plant tissue can be altered due to external environmental factors such as diseases, causing changes in tissue color, leaf shape, transpiration rate, leaf morphology and density, which leads to modified optical properties in the leaf tissue, altering its spectral response [33,34]. The composition and content of pigments are modified when leaves are exposed to pathogens that cause chlorotic and necrotic symptoms [34], such as target spot.

In the visible range (VIS) between wavelengths 400 and 700 nm, there is low reflectance of the canopy due to the absorption of chlorophyll and other pigments [35], as shown in the reference table, where the visible region is more closely related to photosynthesizing pigments such as chlorophyll, anthocyanins, and carotenes. Therefore, this range can be used to detect changes in leaf color caused by diseases and stress in plants [36]. The low reflectance in the visible spectrum range is indicative of the efficiency of these photosynthesizing pigments in absorbing light to sustain the essential metabolic activities of plants and the higher reflectance of the plants affected by the disease is due to the damage caused to the pigments, negatively affecting their function in the plant and altering their reflectance in this range [37]. This relationship between reflectance and photosynthetic pigments provides important information for understanding the physiological conditions and the state of the health of the plants.

In the visible range, reflectance increases in proportion to the severity of the disease. However, in the near-infrared (NIR) region, higher reflectance is observed in healthier leaves [38]. Overall, healthy plants have low reflectance in the visible and mid-infrared regions and high reflectance in the NIR [39], This pattern of reflectance in the spectral regions provides valuable indications of the plant's phytosanitary condition, and is particularly relevant for plant health assessments and early detection of diseases. This behavior was partially observed in the hyperspectral signatures in Figure 3, with the exception of the 725–863 nm band, where there was a peak of reflectance in healthy leaves similar to leaves with a 25% severity level.

Changes observed in the spectral signature at 25% severity when compared to healthy leaves can provide early information on the biochemical changes in the leaf caused by the disease, and the use of a hyperspectral sensor is essential for implementing effective strategies to diagnose target spot and prevent major crop losses [36]. Furthermore, VIs calculated from the reflectance of the VIS and NIR bands can provide more accurate estimates of chlorophyll content, ensuring accurate results regarding the plant's photosynthetic activity [40].

In the SWIR region, a higher reflectance is remarkable at the highest level of disease severity, as this band is associated with the leaf's chemical composition and water content [41,42]. Several studies have reported an increased reflectance in the SWIR region in leaves with a higher severity of diseases such as powdery mildew, grapevine leafroll virus and rust as a result of water loss through the lesions [42–44].

Detecting, identifying and quantifying plant diseases using sensors allows more appropriate management, as the sensors are sensitive, accurate and easy to use for evaluating diseases [45]. Choosing the sensor to use will depend on the resources available, since multispectral sensors are easier to acquire from an economic point of view. By canonical analysis, it can be seen that the multispectral sensor had a higher relationship between healthy leaves and grain weight, both close to the VIs SAVI and EVI, and the 840 nm wavelength. Thus, using this sensor for obtaining these VIs is more sensitive for estimating possible yields in healthy plants due to its higher proximity to grain weight.

There was a behavior in which healthy leaves had a higher association with NDRE and GNDVI when the hyperspectral sensor was used. Using vegetation indices from calculations on the VIS/NIR range can be efficient in agricultural disease monitoring, and can detect changes in vegetation caused by disease attack [3].

Leaves with 25% severity were close to the 680–750 nm range, equivalent to B5, and the 1460–1650 nm range, equivalent to B9. The stronger relationship between these spectral bands and the lower severity of the disease enables early identification of target spot. The hyperspectral sensor deserves to be highlighted in this relationship with lower disease severity levels because plants with a 25% level are still unable to see symptoms in the upper third, making it difficult for the multispectral sensor to capture differences.

The most severely attacked leaves were in the 435–470 nm, 1850–1930 nm, and 2130–2460 nm bands, where Figure 3 shows an increased reflectance in these bands in the hyperspectral signature. The 435–470 bands belong to the visible region, which have a higher relevance for classifying the disease, as they are directly related to the pigment absorption regions, which suffer disturbances characterized by chlorosis when the disease is present [10]. The SWIR region covering the 1850–1930 and 2130–2460 bands tends to increase its reflectance when the leaf's internal water content decreases, which is directly related to a higher disease infection rate [46].

Once the disease severities had been distinguished spectrally, this information was used in machine learning models to find accurate algorithms for classifying disease severity. Overall, the algorithms showing the best results for the three metrics were LR and SVM using reflectance, i.e., using all the information from the spectral range provided by the sensor. The authors of [47] found high accuracy values in the classification of diseased and healthy leaves by using the SVM algorithm, similarly to [44], who used LR to find a disease detection model. The SVM has been proven to be an effective algorithm in several classification tasks, such as classifying soybean genotypes regarding the primary macronutrient contents [48] and classifying soybean genotypes according to their content of industrial grain parameters [10]. In both studies, using the raw information provided by the sensor guaranteed better results for the algorithm. Here, both algorithms had better accuracies using all the information provided by the hyperspectral sensors. Hyperspectral data provide a detailed characterization of the object studied, allowing the assimilation of specific spectral variations for detecting diseases and according to the specifications of each severity level for each disease [49].

Using hyperspectral sensors allowed a more comprehensive acquisition of information across the leaf spectrum, taking into account the different severity levels. This is because hyperspectral sensors allow information about the chemical properties of what is being evaluated to be obtained, enabling the identification, detection and analysis of the chemical composition of the material, in our case related to the physiology of the plant, facilitating various activities in agriculture and an essential role in harvest monitoring and planning [50]. In our study, this in-depth spectral analysis offers a more detailed understanding of leaf conditions at different severity levels, contributing significantly to the accuracy and sensitivity of plant-health assessments. Using this advanced approach represents remarkable progress in monitoring and diagnostic abilities, with promising implications for management and decision-making in agricultural and environmental contexts.

5. Conclusions

Applying the methodology used in this research and expanding it to other phytosanitary problems in different crops is a promising perspective for advancing disease monitoring in agriculture. In this way, the approach allows the development of broader strategies for monitoring and controlling diseases in various agricultural crops using hyperspectral data and machine learning, thus enabling the expansion of these discoveries for accurate and even early diagnosis of diseases. The discovery of the algorithm that deals better with the task of classifying target stain severity levels makes it possible to use it in an unsupervised way to classify the disease when its severity is unknown to the professional, making the process more assertive for making decisions on the management strategy to be carried out.

In addition to the relevant findings provided by hyperspectral data, the employment of machine learning algorithms provided significant classification performance, achieving

high accuracy in identifying different levels of disease severity. This robust performance suggests that both LR and SVM algorithms are effective, especially when using all available information from the spectral range provided by the sensor to classify target spot severity in soybeans.

Hyperspectral sensors allowed greater acquisition of information across the spectrum of leaves with different levels of severity of the target spot disease. Our results reveal that the LR and SVM algorithms provide high classification accuracy and are therefore best suited for identifying disease severity levels in soybean using the entire reflectance range of the plants.

Author Contributions: Conceptualization, J.D.d.Q.O. and D.C.S.; methodology, F.H.R.B.; software, D.C.S. validation, F.H.R.B., P.E.T. and G.d.F.T.; formal analysis, D.C.S.; investigation, J.D.d.Q.O.; resources, P.E.T. and L.P.R.T.; data curation, P.E.T.; writing—original draft preparation, J.D.d.Q.O.; writing—review and editing, D.C.S. and F.H.R.B.; visualization, J.T.d.O., I.C.d.O., and C.A.d.S.J.; supervision, F.H.R.B.; project administration, P.E.T.; funding acquisition, P.E.T. All authors have read and agreed to the published version of the manuscript.

Funding: Universidade Federal de Mato Grosso do Sul (UFMS), Universidade do Estado do Mato Grosso (UNEMAT), Conselho Nacional de Desenvolvimento Científico e Tecnológico (CNPq)—Grant numbers 303767/2020-0, 309250/2021-8, 306022/2021-4 and 304979/2022-8, and Fundação de Apoio ao Desenvolvimento do Ensino, Ciência e Tecnologia do Estado de Mato Grosso do Sul (FUNDECT) TO numbers 88/2021, 07/2022, 318/2022 and 94/2023, and SIAFEM numbers 30478, 31333, 32242 and 33111. This study was financed in part by the Coordenação de Aperfeiçoamento de Pessoal de Nível Superior—Brazil (CAPES)—Financial Code 001.

Data Availability Statement: Data are available from the corresponding author on reasonable request.

Acknowledgments: The authors would like to thank the Universidade Federal de Mato Grosso do Sul (UFMS), Universidade do Estado do Mato Grosso (UNEMAT), Conselho Nacional de Desenvolvimento Científico e Tecnológico (CNPq).

Conflicts of Interest: The authors declare no conflicts of interest.

References

1. Zhao, M.; Dong, Y.; Huang, W.; Ruan, C.; Guo, J. Regional-Scale Monitoring of Wheat Stripe Rust Using Remote Sensing and Geographical Detectors. *Remote Sens.* **2023**, *15*, 4631.
2. Chen, H.; Li, H.; Liu, Z.; Zhang, C.; Zhang, S.; Atkinson, P.M. A Novel Greenness and Water Content Composite Index (GWCCI) for Soybean Mapping from Single Remotely Sensed Multispectral Images. *Remote Sens. Env.* **2023**, *295*, 113679. https://doi.org/10.1016/j.rse.2023.113679.
3. Arantes, B.H.T.; Martins, G.D.; Carvalho, E.R.; Nogueira, L.C.A. Identificação de Ferrugem Na Soja Por Meio de Imagens de Alta Resolução Espacial. *Rev. Bras. Geogr. Física* **2019**, *12*, 1003–1016.
4. Zhang, S.-L.; Sun, Q.; Cao, Y.; Ji, Y.-P.; Zhang, Y.-J.; Herrera-Balandrano, D.D.; Chen, X.; Shi, X.-C.; Wang, S.-Y.; Laborda, P. Biocontrol of Corynespora Cassiicola in Soybean Using a New Phenethyl Alcohol-Producing Meyerozyma Caribbica Strain. *Biol. Control* **2023**, *184*, 105287. https://doi.org/10.1016/j.biocontrol.2023.105287.
5. Edwards Molina, J.P.; Paul, P.A.; Amorim, L.; Da Silva, L.; Siqueri, F.V.; Borges, E.P.; Campos, H.D.; Venancio, W.S.; Meyer, M.C.; Martins, M.C. Effect of Target Spot on Soybean Yield and Factors Affecting This Relationship. *Plant Pathol.* **2019**, *68*, 107–115.
6. Dixon, L.J.; Schlub, R.L.; Pernezny, K.; Datnoff, L.E. Host Specialization and Phylogenetic Diversity of Corynespora Cassiicola. *Phytopathology* **2009**, *99*, 1015–1027.
7. Sumabat, L.G.; Kemerait, R.C., Jr.; Brewer, M.T. Phylogenetic Diversity and Host Specialization of Corynespora Cassiicola Responsible for Emerging Target Spot Disease of Cotton and Other Crops in the Southeastern United States. *Phytopathology* **2018**, *108*, 892–901.
8. Aguiar, F.M.; Vallad, G.E.; Timilsina, S.; Veloso, J.S.; Fonseca, M.E.N.; Boiteux, L.S.; Reis, A. Phylogenetic Network Analysis of South and North American Corynespora Cassiicola Isolates from Tomato, Cucumber, and Novel Hosts. *Eur. J. Plant Pathol.* **2022**, *163*, 657–671.
9. Yamamoto, S.; Nomoto, S.; Hashimoto, N.; Maki, M.; Hongo, C.; Shiraiwa, T.; Homma, K. Monitoring Spatial and Time-Series Variations in Red Crown Rot Damage of Soybean in Farmer Fields Based on UAV Remote Sensing. *Plant Prod. Sci.* **2023**, *26*, 36–47.
10. Bajwa, S.G.; Rupe, J.C.; Mason, J. Soybean Disease Monitoring with Leaf Reflectance. *Remote Sens.* **2017**, *9*, 127.
11. Shahi, T.B.; Xu, C.-Y.; Neupane, A.; Guo, W. Recent Advances in Crop Disease Detection Using UAV and Deep Learning Techniques. *Remote Sens.* **2023**, *15*, 2450.

12. Anderson, K.; Gaston, K.J. Lightweight Unmanned Aerial Vehicles Will Revolutionize Spatial Ecology. *Front. Ecol. Env.* **2013**, *11*, 138–146.
13. Colomina, I.; Molina, P. Unmanned Aerial Systems for Photogrammetry and Remote Sensing: A Review. *ISPRS J. Photogramm. Remote Sens.* **2014**, *92*, 79–97.
14. Farber, C.; Mahnke, M.; Sanchez, L.; Kurouski, D. Advanced Spectroscopic Techniques for Plant Disease Diagnostics. A Review. *Trends Anal. Chem.* **2019**, *118*, 43–49.
15. Koc, A.; Odilbekov, F.; Alamrani, M.; Henriksson, T.; Chawade, A. Predicting Yellow Rust in Wheat Breeding Trials by Proximal Phenotyping and Machine Learning. *Plant Methods* **2022**, *18*, 30. https://doi.org/10.1186/s13007-022-00868-0.
16. dos Santos, H.G.; JACOMINE, P.K.T.; Dos Anjos, L.H.C.; De Oliveira, V.A.; LUMBRERAS, J.F.; COELHO, M.R.; De Almeida, J.A.; de Araujo Filho, J.C.; De Oliveira, J.B.; CUNHA, T.J.F. *Sistema Brasileiro de Classificação de Solos*; Embrapa: Brasília, Brazil, 2018; ISBN 8570358172.
17. Soja, E.; Dinali, C.; Seixas, S.; Alvadi, N.N.; Balbinot, A.; Francisco, J.; Krzyzanowski, C.; Villas, R.M.; De, B.; Leite, C.; et al. *Sistemas de Produção 17 Tecnologias de Produção de Soja*; Embrapa Soja: Londrina, Brazil, 2020.
18. Soares, R.M.; Godoy, C.V.; Oliveira, M.C.N. de Escala Diagramática Para Avaliação Da Severidade Da Mancha Alvo Da Soja. *Trop. Plant Pathol.* **2009**, *34*, 333–338.
19. da Silva Junior, C.A.; Nanni, M.R.; Shakir, M.; Teodoro, P.E.; de Oliveira-Júnior, J.F.; Cezar, E.; de Gois, G.; Lima, M.; Wojciechowski, J.C.; Shiratsuchi, L.S. Soybean Varieties Discrimination Using Non-Imaging Hyperspectral Sensor. *Infrared Phys. Technol.* **2018**, *89*, 338–350. https://doi.org/10.1016/j.infrared.2018.01.027.
20. Rouse, J.W.; Haas, R.H.; Schell, J.A.; Deering, D.W. Monitoring Vegetation Systems in the Great Plains with ERTS. *NASA Spec. Publ.* **1974**, *351*, 309.
21. Gitelson, A.; Merzlyak, M.N. Spectral Reflectance Changes Associated with Autumn Senescence of Aesculus Hippocastanum L. and Acer Platanoides L. Leaves. Spectral Features and Relation to Chlorophyll Estimation. *J. Plant Physiol.* **1994**, *143*, 286–292. https://doi.org/10.1016/S0176-1617(11)81633-0.
22. Huete, A.R. A Soil-Adjusted Vegetation Index (SAVI). *Remote Sens. Environ.* **1988**, *25*, 295–309. https://doi.org/10.1016/0034-4257(88)90106-X.
23. Gitelson, A.A.; Merzlyak, M.N. Signature Analysis of Leaf Reflectance Spectra: Algorithm Development for Remote Sensing of Chlorophyll. *J. Plant Physiol.* **1996**, *148*, 494–500. https://doi.org/10.1016/S0176-1617(96)80284-7.
24. Perry, E.M.; Goodwin, I.; Cornwall, D. Remote Sensing Using Canopy and Leaf Reflectance for Estimating Nitrogen Status in Red-Blush Pears. *HortScience Horts.* **2018**, *53*, 78–83. https://doi.org/10.21273/HORTSCI12391-17.
25. Egmont-Petersen, M.; de Ridder, D.; Handels, H. Image Processing with Neural Networks—A Review. *Pattern Recognit.* **2002**, *35*, 2279–2301. https://doi.org/10.1016/S0031-3203(01)00178-9.
26. Quinlan, J.R. C4. 5: Programming for Machine Learning. *Morgan Kauffmann* **1993**, *38*, 49.
27. Štepanovský, M.; Ibrová, A.; Buk, Z.; Velemínská, J. Novel Age Estimation Model Based on Development of Permanent Teeth Compared with Classical Approach and Other Modern Data Mining Methods. *Forensic Sci. Int.* **2017**, *279*, 72–82. https://doi.org/10.1016/j.forsciint.2017.08.005.
28. Al Snousy, M.B.; El-Deeb, H.M.; Badran, K.; Al Khlil, I.A. Suite of Decision Tree-Based Classification Algorithms on Cancer Gene Expression Data. *Egypt. Inform. J.* **2011**, *12*, 73–82. https://doi.org/10.1016/j.eij.2011.04.003.
29. Belgiu, M.; Drăguţ, L. Random Forest in Remote Sensing: A Review of Applications and Future Directions. *ISPRS J. Photogramm. Remote Sens.* **2016**, *114*, 24–31. https://doi.org/10.1016/j.isprsjprs.2016.01.011.
30. Kalmegh, S. *Analysis of WEKA Data Mining Algorithm REPTree, Simple Cart and RandomTree for Classification of Indian News*; Academia Inc.: San Francisco, CA, USA, 2015; Volume 2.
31. Nalepa, J.; Kawulok, M. Selecting Training Sets for Support Vector Machines: A Review. *Artif. Intell. Rev.* **2019**, *52*, 857–900. https://doi.org/10.1007/s10462-017-9611-1.
32. Bhering, L.L. Rbio: A Tool for Biometric and Statistical Analysis Using the R Platform. *Crop Breed. Appl. Biotechnol.* **2017**, *17*, 187–190.
33. West, J.S.; Bravo, C.; Oberti, R.; Moshou, D.; Ramon, H.; McCartney, H.A. Detection of Fungal Diseases Optically and Pathogen Inoculum by Air Sampling. In *Precision Crop Protection—The Challenge and Use of Heterogeneity*; Springer Dordrecht: Dordrecht, The Netherlands, 2010; pp. 135–149.
34. Mahlein, A.-K. Plant Disease Detection by Imaging Sensors–Parallels and Specific Demands for Precision Agriculture and Plant Phenotyping. *Plant Dis.* **2016**, *100*, 241–251.
35. Christenson, B.S.; Schapaugh, W.T., Jr.; An, N.; Price, K.P.; Fritz, A.K. Characterizing Changes in Soybean Spectral Response Curves with Breeding Advancements. *Crop Sci.* **2014**, *54*, 1585–1597. https://doi.org/10.2135/cropsci2013.08.0575.
36. Zahir, S.A.D.M.; Omar, A.F.; Jamlos, M.F.; Azmi, M.A.M.; Muncan, J. A Review of Visible and Near-Infrared (Vis-NIR) Spectroscopy Application in Plant Stress Detection. *Sens. Actuators A Phys.* **2022**, *338*, 113468. https://doi.org/10.1016/j.sna.2022.113468.
37. Moreira, M.A. *Fundamentos Do Sensoriamento Remoto e Metodologias de Aplicação*; 3º Edição; UFV: Chilliwack, BC, Canada, 2005.
38. Negrisoli, M.M.; Negrisoli, R.; da Silva, F.; Lopes, L.S.; de Souza Júnior, F.S.; Velini, E.D.; Carbonari, C.A.; Rodrigues, S.A.; Raetano, C.G. Soybean Rust Detection and Disease Severity Classification by Remote Sensing. *Agron. J.* **2022**, *114*, 3246–3262. https://doi.org/10.1002/agj2.21152.
39. Ahmed, M.; Seraj, R.; Islam, S.M.S. The K-Means Algorithm: A Comprehensive Survey and Performance Evaluation. *Electronics* **2020**, *9*, 1295.

40. Saravia, D.; Salazar, W.; Valqui-Valqui, L.; Quille-Mamani, J.; Porras-Jorge, R.; Corredor, F.-A.; Barboza, E.; Vásquez, H.V.; Casas Diaz, A.V.; Arbizu, C.I. Yield Predictions of Four Hybrids of Maize (*Zea mays*) Using Multispectral Images Obtained from UAV in the Coast of Peru. *Agronomy* **2022**, *12*, 2630.
41. Carter, G.A.; Knapp, A.K. Leaf Optical Properties in Higher Plants: Linking Spectral Characteristics to Stress and Chlorophyll Concentration. *Am. J. Bot.* **2001**, *88*, 677–684.
42. Junges, A.H.; Almança, M.A.K.; Fajardo, T.V.M.; Ducati, J.R. Leaf Hyperspectral Reflectance as a Potential Tool to Detect Diseases Associated with Vineyard Decline. *Trop Plant Pathol.* **2020**, *45*, 522–533. https://doi.org/10.1007/s40858-020-00387-0.
43. Knauer, U.; Matros, A.; Petrovic, T.; Zanker, T.; Scott, E.S.; Seiffert, U. Improved Classification Accuracy of Powdery Mildew Infection Levels of Wine Grapes by Spatial-Spectral Analysis of Hyperspectral Images. *Plant Methods* **2017**, *13*, 47.
44. Heim, R.H.J.; Wright, I.J.; Chang, H.; Carnegie, A.J.; Pegg, G.S.; Lancaster, E.K.; Falster, D.S.; Oldeland, J. Detecting Myrtle Rust (*Austropuccinia psidii*) on Lemon Myrtle Trees Using Spectral Signatures and Machine Learning. *Plant Pathol.* **2018**, *67*, 1114–1121.
45. Mahlein, A.-K.; Oerke, E.-C.; Steiner, U.; Dehne, H.-W. Recent Advances in Sensing Plant Diseases for Precision Crop Protection. *Eur. J. Plant Pathol.* **2012**, *133*, 197–209. https://doi.org/10.1007/s10658-011-9878-z.
46. de Oliveira Pires, M.S.; de Carvalho Alves, M.; Pozza, E.A. Multispectral Radiometric Characterization of Coffee Rust Epidemic in Different Irrigation Management Systems. *Int. J. Appl. Earth Obs. Geoinf.* **2020**, *86*, 102016. https://doi.org/10.1016/j.jag.2019.102016.
47. Bose, P.; Dutta, S.; Goyal, V.; Bandyopadhyay, S.K. Leaf Diseases Detection of Medicinal Plants Based on Support Vector Machine Classification Algorithm. *J. Pharm. Res. Int.* **2021**, *33*, 111–119.
48. Santana, D.C.; Teixeira Filho, M.C.M.; da Silva, M.R.; das Chagas, P.H.M.; de Oliveira, J.L.G.; Baio, F.H.R.; Campos, C.N.S.; Teodoro, L.P.R.; da Silva Junior, C.A.; Teodoro, P.E. Machine Learning in the Classification of Soybean Genotypes for Primary Macronutrients' Content Using UAV–Multispectral Sensor. *Remote Sens.* **2023**, *15*, 1457.
49. da Silva Barros, P.P.; Rosalen, D.L.; Iost Filho, F.H.; Martins, G.D.; Di Leo, N. Monitoramento Fitossanitário Utilizando Sensoriamento Remoto: Avanços e Desafios. *Rev. Bras. Cart.* **2021**, *73*, 489.
50. Gewali, U.B.; Monteiro, S.T.; Saber, E. Machine Learning Based Hyperspectral Image Analysis: A Survey. *arXiv* **2018**, arXiv:1802.08701.